
RESCAST-100K: A Comprehensive Dataset for Cross-Domain Residential Load and Indoor Temperature Forecasting

Jainam Dhruva

Department of Computer Science
University of Kentucky
Lexington, KY 40506
jainam.dhruva@uky.edu

Yousaf Raza

Department of Computer Science
University of Kentucky
Lexington, KY 40506
yra237@uky.edu

A.B Siddique

Department of Computer Science
University of Kentucky
Lexington, KY 40506
msi.290@g.uky.edu

Simone Silvestri

Department of Computer Science
University of Kentucky
Lexington, KY 40506
simone.silvestri@uky.edu

Abstract

Accurate short-term forecasting of residential energy load and indoor temperature is essential for home energy management systems, grid-level demand response participation, and community-level energy efficiency programs. Domain adaptation methods and transfer learning have shown promise in improving forecasting accuracy under data heterogeneity and scarcity scenarios commonly observed at the residential level. However, progress remains limited by the absence of comprehensive residential datasets: existing ones are narrow in target coverage and lack structured support for cross-domain evaluation. To address this, we introduce RESCAST-100K, a large-scale residential forecasting benchmark for studying cross-domain generalization. It exposes a configuration-driven interface that instantiates source and target domains along interpretable axes, such as geography, climate zone, wall construction, and heating equipment, supporting systematic evaluation of transfer learning, domain adaptation, and zero-shot generalization under controlled domain shifts. The benchmark covers approximately 100,000 EnergyPlus-simulated U.S. homes derived from ResStock, providing 15-minute time series of three coupled targets per home, namely total load, HVAC (heating, ventilation, and air conditioning) load, and indoor temperature, together with weather channels, HVAC setpoints, and over 40 static building covariates. Finally, it integrates five real-world residential datasets under a unified schema, supporting sim-to-real evaluation on the same tasks. We benchmark models from recurrent, attention, and MLP-mixer architectures for zero-shot performance across different domains, under missing input data conditions, for each task. Cross-attention and MLP-mixer based models consistently outperform recurrent and classical transformer-based baselines under domain shift. RESCAST-100K is intended to support the machine learning and building analytics communities in advancing cross-domain residential forecasting at the home, community, and grid levels.

1 Introduction

Accurate short-term forecasting of residential energy load and indoor temperature is critical for modern data-driven energy systems, enabling applications such as intelligent home energy management, grid balancing, and demand response [19, 23, 16, 59]. Recent advances in deep learning have improved forecasting accuracy substantially, but these models typically require access to large amounts of historical training data from the target domain [2, 56, 39]. Residential settings rarely meet this requirement: data is often scarce, fragmented, or privacy-sensitive, motivating forecasting models that generalize across domains.

Residential environments exhibit multi-dimensional heterogeneity across geographic location, climate, building envelope, and HVAC systems, where each axis induces a distinct distribution shift for total load, HVAC load, and indoor temperature forecasting. Domain adaptation and transfer learning have emerged as promising approaches under such heterogeneity [17, 38, 19]. Despite this growing interest, progress remains hindered by the lack of large-scale datasets that support systematic evaluation under controlled domain shifts. Existing datasets are limited in one or more aspects: they focus on non-residential buildings, omit key exogenous variables such as weather or control signals, lack targets such as HVAC load or indoor temperature, or do not span enough diversity to study generalization [17, 6, 43, 36]. Moreover, prior benchmarks rarely integrate synthetic and real-world data under a unified schema, making sim-to-real evaluation difficult.

Table 1: Comparison of RESCAST-100K with existing building energy and temperature datasets. Categories are grouped into *Scope*, *Targets*, *Covariates*, and *Cross-Domain Support*. ✓ = supported, ✗ = not supported, and ~ = partial / limited. “Resi.” = residential.

Dataset	Scope		Targets			Covariates			Cross-Domain Support				
	Resi. focus	Open access	Total load	HVAC load	Indoor temp.	Weather channels	Control setpoints	Static covs.	Geo. split	Climate split	Envel. split	HVAC split	Sim+Real
UCI Electricity [53]	~	✓	✓	✗	✗	✗	✗	✗	✗	✗	✗	✗	✗
Ind. Household Power [25]	✓	✓	✓	✗	✗	✗	✗	✗	✗	✗	✗	✗	✗
Low Carbon London [47]	✓	✓	✓	✗	✗	✗	✗	✗	✗	✗	✗	✗	✗
Pecan Street [1]	✓	✗	✓	~	✗	✗	✗	~	✓	~	✗	✗	✗
Ecobee DYD [34]	✓	✗	✗	✗	✓	~	✓	~	~	~	✗	✗	✗
BDG2 [36]	✗	✓	✓	✗	✗	✓	✗	~	✓	✓	✗	✗	✗
LBNL Bldg. 59 [33]	✗	✓	✓	✓	✓	✓	✓	~	✗	✗	✗	✗	✗
BTS [43]	✗	✓	✓	~	✓	✓	✓	~	✗	✗	✗	✗	✗
BuildingsBench [17]	~	✓	✓	✗	✗	~	✗	~	✓	~	✗	✗	✓
RESCAST-100K (Ours)	✓	✓	✓	✓	✓	✓	✓	✓	✓	✓	✓	✓	✓

To address these limitations, we introduce RESCAST-100K, a large-scale dataset and benchmark for cross-domain residential forecasting. The dataset contains 15-minute resolution time series for over 100,000 homes across the United States, including total load, HVAC load, and indoor temperature, along with rich exogenous variables such as weather and control inputs, and static building covariates. It integrates high-fidelity physics-based simulations with curated real-world datasets under a unified schema, enabling both controlled experimentation and realistic evaluation scenarios.

A key feature of RESCAST-100K is its configuration-driven domain abstraction, which allows users to define domain splits along multiple interpretable axes, including but not limited to, geography, climate zone, construction type, and HVAC technology. This facilitates systematic evaluation of timely methods within transfer learning, meta-learning, domain adaptation, and zero-shot generalization under diverse distribution shifts. Additionally, the combination of synthetic and real data enables study of synthetic-to-real transfer, which is essential for scaling methods in data-constrained environments.

Using this benchmark, we evaluate commonly used and state of the art time-series models, including recurrent, transformer-based, and mixer-style architectures, under both standard and missing-covariate settings. Our results demonstrate that cross-attention and MLP-mixer based models retain best accuracy under domain shift across all three forecasting tasks. These two architectures also achieve the best sim-to-real probabilistic forecasting accuracy.

Overall, this work makes the following contributions:

- We introduce RESCAST-100K, a large-scale residential dataset of 100K homes with a configuration-driven interface that enables controlled study of cross-domain forecasting along axes such as geography, climate zone, construction type, and heating equipment.
- The dataset provides multiple coupled targets — total load, HVAC load, and indoor temperature — essential for downstream tasks, together with exogenous features including weather variables, HVAC setpoints, and static covariates characterizing each home.
- We benchmark recurrent, attention, and MLP-mixer style models and provide insights for model-architecture choices. We further integrate synthetic and real-world datasets under a unified schema and provide zero shot sim-to-real evaluations.

2 Related Work

Current Datasets. Public and open source datasets of building operational data have been scarce, narrow in scope, leave out on information-rich co variates, or are often inaccessible for reproducible research. Aggregate consumption datasets such as the UCI Electricity Load Diagrams [53], Low Carbon London dataset [47], and the Individual Household Electric Power Consumption dataset [25], common in machine learning and time series benchmarking, provide hourly or sub-hourly load measurements; but they are restricted to a single channel of total electricity demand without coupled weather, control, or information about the homes. Some larger datasets such as the Building Data Genome Project 2 (BDG2) [36, 35] aggregate 3053 meters across 1636 buildings, while the Building Performance Database [28] catalogs over a million buildings; however, both remain dominated by commercial stock, rely on coarse temporal resolutions, and/or also do not include relevant covariates. BuildingsBench [17] releases Buildings-900K, a simulated corpus of buildings derived from Resstock for enabling pretraining of energy forecasting models. But this dataset lacks granular information, does not capture exogenous features, lacks HVAC load and indoor temperature target series essential for energy management systems, and does not support systematic cross domain adaptation. On the contrary, some holistic datasets such as Lawrence Berkeley National Laboratory’s Building 59 (LBNL59) [33] and the Building TimeSeries (BTS) dataset [43] expose comprehensive operational signals—including HVAC states, setpoints, and zone temperatures—but represent only one and three buildings, respectively, severely limiting their utility for studying generalization across domains. Other resources, such as Pecan Street [1], are either gated, exclude important exogenous features, or are restricted to specific geographies.

Scaling Through Simulations. To overcome the scaling limits of real-world data, recent work has turned to high-fidelity physics-based simulation. The U.S. Department of Energy’s ResStock [51] and ComStock [41] provide statistically representative models of U.S. residential and commercial stock, calibrated against advanced metering data and surveys such as CBECS [15]. Models pre-trained on synthetic corpora generated by simulators such as EnergyPlus have shown preliminary success in generalizing to real buildings in both zero-shot and fine-tuned settings [17, 18, 60, 45], and sim-to-real transfer is helpful in the residential setting, where smart-meter and smart-thermostat data are scarce due to collection cost and privacy concerns [52, 29]. But most efforts predominantly target commercial buildings, and sim-to-real transfer for residential households remains underexplored, due to higher heterogeneity and limited structured real-world data [17, 52].

Forecasting in Residential Setting. Several works have focused on developing better models for improving forecasting within residential domain. The problem has been shown to be particularly challenging as household loads are strongly influenced by stochastic occupant behavior, appliance usage, weather, envelope properties, equipment type, and thermostat operation [61, 9, 37, 31]. Previous works have benchmarked transformer style and Mixer style model architectures for time series forecasting such as Informer [62], PatchTST [39], TSMixer [11], and TimeXer [56]. However, most evaluations focus on univariate-input based forecasting, focus on non-residential setting, and primarily lack cross domain generalization benchmarking of these approaches [46, 17, 50]. Models trained on one population of homes may fail under shifts in geography, climate zone, construction type, heating and cooling equipment, occupancy pattern, or data availability [58, 46, 61, 38].

Cross-Domain Generalization in Residential Buildings. Transfer learning has emerged as a principal approach to scalable deployment of data-driven controllers and forecasters across buildings, given the prohibitive cost of per-building data collection and customization. Reinforcement learning based methods in HVAC-control studies include Xu et al. [59], Coraci et al. [13], and Lissa et

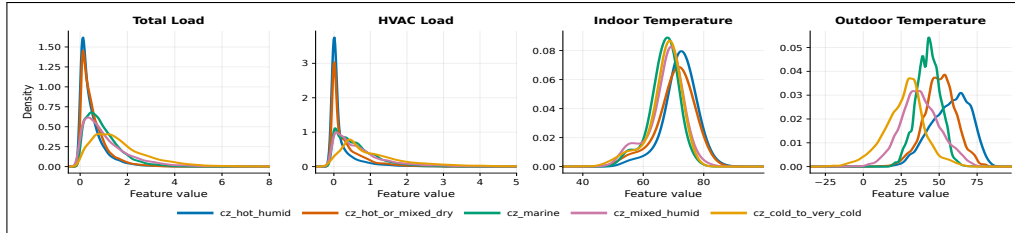


Figure 1: Distribution of total load (kWh), HVAC load (kWh), indoor temperature ($^{\circ}$ F), and outdoor temperature ($^{\circ}$ F) across the five ASHRAE/IECC climate-zone domains: Hot-Humid, Hot/Mixed-Dry, Marine, Mixed-Humid and Cold/Very-Cold. Distributions are estimated via kernel density across all homes within each climate-zone domain. The observed shifts in target-variable distributions indicate cross-domain heterogeneity. When coupled with exogenous covariates and temporal dependencies, these shifts further increase across the domains.

al. [32], who transfer control policies across buildings, room, and microgrid-level heat-pump control. However, model based approaches remain preferred in the building community due to their inherent nature of being more explainable. Model based methods have investigated meta-learning approaches such as MAML [20] and its forecasting extensions [24]. Some other work have evaluated target domain adaptation for residential total load, HVAC load, and indoor temperature forecasting, using Graph Neural Networks [49], Long Short Term Memory models [27], and Transformers [55], under different source and target set cardinalities, but on smaller, individual, and/or non-public datasets [57, 61, 22, 46]. These works focus on smaller domain perturbations under individual and/or non-public dataset, making it difficult to compare the cross-domain generalization efficacy of those approaches.

RESCAST-100K. RESCAST-100K is purpose-built to close gaps observed in recent literature. This comprehensive dataset multi-target timeseries data for approximately 100,000 homes across all U.S. states with paired weather, setpoints, and metadata; integrates five real residential datasets under a consistent schema; and exposes a configuration-based interface for instantiating cross-domain splits. Hence, RESCAST-100K enables transfer-learning, domain-adaptation, zero-shot, and sim-to-real evaluations that prior residential forecasting resources could not support.

3 Dataset Description

Overview. We introduce the RESCAST-100K dataset, for cross domain forecasting in residential setting. Our dataset provides a 15-minute granular view where total load, HVAC load, and the indoor temperature data are coupled with exogenous features and static covariates (refer section A). The exogenous features allow to better capture the patterns in the target. The static variables provide information that can be used for generalization by the model, as well as to evaluate the transferability proxy from one building to another.

Curation. We construct the dataset with a pipeline built on ResStock and EnergyPlus, executed on high-performance computing nodes. ResStock [51] provides a statistically representative distribution of U.S. housing — envelope types, regions, occupancy schedules, and equipment — calibrated against research studies, census records, and surveys [15, 10]. This is paired with approximately 9,000 TMY3 (typical meteorological year) weather files covering the United States. The homes are then conditionally sampled together with their corresponding weather files to produce simulation inputs for roughly 100,000 buildings across the United States. To prevent under-representation of demographically smaller or data-scarce regions, we enforce a near-uniform allocation of approximately 2,000 homes per state. To obtain the target time series, we simulate one year of operation per home in EnergyPlus [40], the U.S. Department of Energy’s reference whole-building simulator. EnergyPlus is the industry standard for building energy modeling, with validation against the ASHRAE Standard 140 method of test for building energy simulation programs [5].

Features and structure. The dataset is sharded into a set of Parquet files, with each consisting of yearly time series data for a batch of homes. The Parquet file contains building ID, timestamps, the three targets (total load, HVAC load, indoor temperature), and the exogenous features. Home

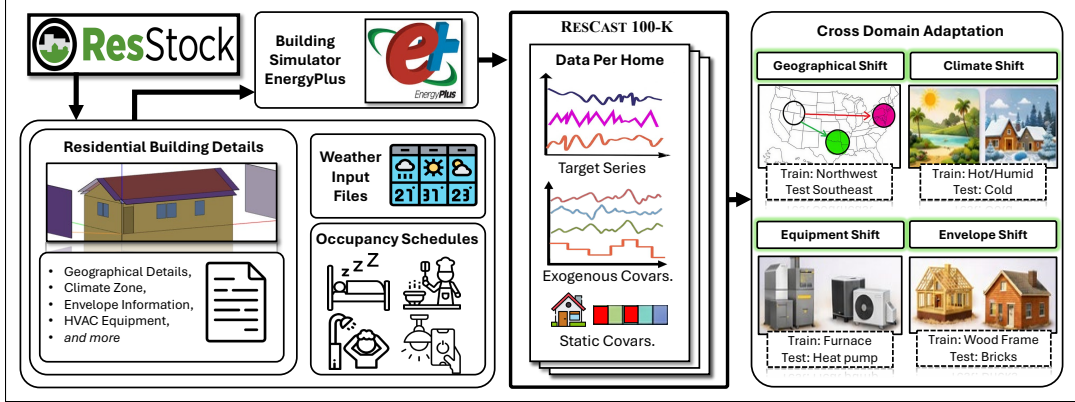


Figure 2: Data Curation pipeline for RESCAST-100K. Home envelope files, weather data, and stochastic schedules, derived from Resstock are used as inputs to EnergyPlus simulations computed through high performance computing (HPC) cluster. The data can be used to create specific domain splits for cross domain adaptations. This dataset can be used to evaluate various domain adaptation methodologies for time series forecasting in residential setting.

properties, i.e., the static covariates — geographical attributes, envelope properties, HVAC system descriptors, etc. — are consolidated into a single parquet file indexed by building ID. To enable sim-to-real evaluation, we include five real residential datasets, summarized in Table 3. Real datasets vary in coverage: some lack weather channels, others omit setpoints, and most expose only a small subset of static home properties. We structure them under a common schema through a combination of automated pre-processing — resampling, outlier removal, and missing-value imputation — and manual intervention to align static-variable definitions across sources.

Table 2: Summary of time series data for each residential dwelling: exogenous covariates, static covariates, and target variables. Files also include respective timesteps for that time series data.

Exogenous features	Static Covariates and Target Features
Outdoor Drybulb temp. ($^{\circ}$ F)	Static properties:
Outdoor Wetbulb temp. ($^{\circ}$ F)	State, Climate zone, Floor area, Wall type,
Relative humidity (%)	Foundation type, HVAC system type, etc.
Wind speed (m/s)	Targets:
Diffuse solar radiation (W/m^2)	Total electric load (kWh)
Direct solar radiation (W/m^2)	HVAC electric load (kWh)
Heating setpoint ($^{\circ}$ F)	Indoor temperature ($^{\circ}$ F)
Cooling setpoint ($^{\circ}$ F)	

Usage. The dataset code provides a configuration-driven data loader that instantiates a domain from a user-defined YAML file. Users specify a domain by listing values along any axis exposed in the metadata: states, cities, climate zones, floor-area ranges, wall types, heating equipment, and so on. We provide a dictionary of domain axes and the categorical values it can consist of. The code provides a Pytorch style dataset and dataloader for source and target domain as defined in the YAML config file. The dataloader handles both synthetic and real datasets and returns PyTorch-compatible iterators, so any user-defined or pre-defined model can be trained and evaluated under identical interfaces. The data curation pipeline and its application are summarized in Figure 2.

4 Problem Statement

RESCAST-100K supports a broad class of residential forecasting problems, including supervised learning, transfer learning, domain adaptation, zero-shot generalization, robustness to missing covariates, and sim-to-real evaluation. Here, we instantiate one representative setting: probabilistic

Table 3: Overview of real datasets included in RESCAST-100K.

Dataset	Indoor temp.	HVAC Load	Total Load	Homes	Static Vars	Geo Locations Represented	Data Time Range
ECOBEE[34]	✓	×	×	954	23	≈ 43 cities	Jan 2017 – Dec 2017
HEAPO[7]	×	×	✓	1,407	9	≈ 1 city	May 2019 – Feb 2024
IDEAL[44]	✓	×	✓	255	19	≈ 5	Aug 2016 – Jun 2018
NEST[26]	✓	✓	✓	1	20	≈ 1 city	Jul 2022 – Jun 2023
REFIT[21]	×	×	✓	20	11	Not available	Sep 2013 – Jul 2015

forecasting under domain transfer, with the goal of minimizing expected forecasting loss across shifted domains while handling missing dynamic and static covariates.

Forecasting setup. We formulate residential forecasting as a univariate forecasting task instantiated independently for each of the three targets (Total, HVAC, Temp.), with multivariate dynamic and static inputs. Let L_c and L_f denote context length and forecast horizon. For each sample i ,

$$\mathbf{x}_{1:L_c}^{(i)} \in \mathbb{R}^{N_p \times L_c}, \quad \mathbf{u}_{1:L_f}^{(i)} \in \mathbb{R}^{N_f \times L_f}, \quad \mathbf{s}^{(i)} \in \mathbb{R}^{N_s}, \quad \mathbf{y}_{1:L_f}^{(i)} \in \mathbb{R}^{1 \times L_f},$$

where $\mathbf{x}_{1:L_c}$ stacks the past target and past covariates (N_p channels), $\mathbf{u}_{1:L_f}$ contains future-known dynamic inputs (N_f channels, e.g., weather forecasts and scheduled setpoints), \mathbf{s} contains static home attributes (N_s entries), and $\mathbf{y}_{1:L_f}$ is the target trajectory. We learn a quantile predictor

$$f_\theta : (\mathbf{x}_{1:L_c}, \mathbf{u}_{1:L_f}, \mathbf{s}) \mapsto \hat{\mathbf{Q}}_\theta \in \mathbb{R}^{L_f \times Q}, \quad (1)$$

where \hat{Q}_{t,τ_q} estimates the τ_q -quantile of Y_t for levels $\tau_1 < \dots < \tau_Q \in (0, 1)$, trained by minimizing the average pinball loss $\mathcal{L}_{\text{prob}}$ over the horizon and quantile grid (Appendix C.1):

$$\min_{\theta} \mathbb{E}_{(\mathbf{x}, \mathbf{u}, \mathbf{s}, \mathbf{y}) \sim P} [\mathcal{L}_{\text{prob}}(f_\theta(\mathbf{x}, \mathbf{u}, \mathbf{s}), \mathbf{y})]. \quad (2)$$

Probabilistic forecasts are essential in residential settings, where downstream control and planning rely on uncertainty quantification [23, 48, 3].

Cross-domain generalization. Homes are drawn from heterogeneous distributions induced by geography, climate, envelope, and equipment. Each domain $d \in \mathcal{D}$ can be modeled with joint $P_d(\mathbf{x}_{1:L_c}, \mathbf{u}_{1:L_f}, \mathbf{s}, \mathbf{y}_{1:L_f})$, defined by fixing values along a designated subset of static attributes (e.g., climate zone, wall type); the remaining static attributes vary within each domain and are passed to f_θ . Given source domains $\mathcal{D}_{\text{src}} = \{d_1, \dots, d_K\}$, training minimizes the expected risk under a meta-distribution Π_{src} corresponding to sample-weighted pooling of source-domain data:

$$\min_{\theta} \mathbb{E}_{d \sim \Pi_{\text{src}}} \mathbb{E}_{(\mathbf{x}, \mathbf{u}, \mathbf{s}, \mathbf{y}) \sim P_d} [\mathcal{L}_{\text{prob}}(f_\theta(\mathbf{x}, \mathbf{u}, \mathbf{s}), \mathbf{y})]. \quad (3)$$

Generalization is assessed zero-shot on a held-out target domain $d^* \notin \mathcal{D}_{\text{src}}$, or with limited adaptation data in the transfer-learning setting. Domain splits are instantiated by the user via a YAML config provided with the dataset.

Missing covariates. In practice, weather channels, setpoints, or home metadata may be systematically absent due to lack of sensing, older thermostat and metering infrastructure, incomplete metadata collection, or inconsistencies across data providers. We model this via a stochastic masking operator $\mathcal{M} \sim \mathcal{P}_M$ that drops complete dynamic channels independently and the static-covariate vector jointly, yielding $(\tilde{\mathbf{x}}, \tilde{\mathbf{u}}, \tilde{\mathbf{s}}) = \mathcal{M}(\mathbf{x}, \mathbf{u}, \mathbf{s})$; and the target is never masked. The full training objective is

$$\min_{\theta} \mathbb{E}_{d \sim \Pi_{\text{src}}} \mathbb{E}_{(\mathbf{x}, \mathbf{u}, \mathbf{s}, \mathbf{y}) \sim P_d} \mathbb{E}_{\mathcal{M} \sim \mathcal{P}_M} [\mathcal{L}_{\text{prob}}(f_\theta(\tilde{\mathbf{x}}, \tilde{\mathbf{u}}, \tilde{\mathbf{s}}), \mathbf{y})]. \quad (4)$$

Thus, our formulation seeks to learn a probabilistic forecaster that generalizes across structured domain shifts while remaining robust to incomplete inputs.

5 Experiments

We benchmark the performance of some of the prominent models today following our problem formulation. Specifically, in this work, we evaluate and compare the zero-shot performance of Encoder LSTM (LSTM-E) [46], Encoder & Decoder LSTM (LSTM) [19], Transformer [55], TimeXer [56], TSMixer [11], and PatchTST [39] models. Some models are further modified to have a robust version, specifically LSTM-R, Transformer-R, and TimeXer-R, and are created to handle unavailable data and provide benchmarks for robust forecasting. For all experiments, our context length - the length of past timesteps used in input - is $L_c = 384$, equivalent to 4 days of data, and we predict $L_f = 96$ timesteps which equivalent to 1 day of data. This context and horizon is consistent with common short-term load residential forecasting settings [17, 2, 24]. The masking operator \mathcal{M} used in our experiments drops *whole input channels* and individual home properties with high probabilities (Appendix C.3). We evaluate forecasting performance using two complementary metrics: Normalized Root Mean Square Error (NRMSE) and Continuous Ranked Probability Score (CRPS), corresponding to evaluating point prediction accuracy and probabilistic prediction accuracy (Appendix C.2).

5.1 In-Domain Evaluation

Firstly, we evaluate the models in-domain with full data availability and observe their accuracy. Then we develop the top four performing model as robust models. Robust models are then evaluated in-domain under conditions where some of the dynamic and static covariates are missing. Here, we consider the past target is always available.

For in domain evaluation, we train models on a data split consisting of homes from US states from all climate zones, and test it on data from the same homes (Appendix B). In-distribution evaluations provide a preliminary understanding of how different models may perform under stronger domain shifts. The results are presented in Table 4.

Table 4: Performance on three forecasting tasks on the US States I dataset, comparing models under full data availability and robust models under missing/unavailable data.

Setting	Model	NRMSE			CRPS		
		Total	HVAC	Temp	Total	HVAC	Temp
Full data availability	LSTM-E	46.47	46.21	2.68	0.143	0.090	0.802
	LSTM	<u>40.39</u>	39.48	3.97	<u>0.128</u>	0.087	1.407
	Transformer	38.64	<u>34.45</u>	3.78	0.121	0.077	1.501
	TSMixer	42.08	35.94	<u>1.19</u>	0.166	0.091	0.364
	TimeXer	40.43	32.56	0.98	0.156	<u>0.081</u>	0.263
	PatchTST	44.02	38.02	1.21	0.147	0.094	<u>0.325</u>
Missing and/or unavailable data (-R: robust models)	LSTM-R	46.84	44.27	5.33	0.191	0.102	2.134
	Transformer-R	48.48	42.42	5.06	0.194	0.098	1.994
	TSMixer-R	<u>43.49</u>	<u>37.29</u>	1.21	0.174	0.094	<u>0.367</u>
	TimeXer-R	42.13	35.11	0.95	0.163	0.086	0.251

We observe transformer and TimeXer perform better when all data is available in-domain. Many works in building analytics community have previously focused on such in-domain setting with full data availability. But under conditions with missing data, TimeXer and TSMixer models consistently out-perform classical transformer and LSTMs. As LSTM, Transformer, TSMixer and TimeXer are the best performing model in-domain, we use their robust variants for the following experiments.

5.2 Cross-Domain Zero-Shot Evaluation

We evaluate how well models generalize when trained on one group of homes and tested on a different group of homes categorized under a specific domain-shift. To do this, we define four *domain categories*, each capturing a distinct axis of heterogeneity in the residential stock: state-based geography (State), ASHRAE climate zone (CZ), wall construction type (Wall), and heating technology (Heating). Within each category, we partition homes into four to five *domain splits*. For example, the State category contains splits for Midwestern, Northeastern, Southern, Mountain West, and South-Central states. Full details of all categories and splits are provided in Section B.

For each category, we run a leave-one-split-out evaluation using the robust model variants. We train on a single split and measure zero-shot accuracy on each of the remaining splits in that category, then repeat with every other split serving as the training source. Each training split draws 400 randomly sampled homes and each test split draws 100 randomly sampled homes. Table 5 reports the mean accuracy across every source–target pair within each category.

Table 5: Forecasting results with standard deviation across total load, HVAC load, and indoor temperature forecasting tasks. Best values are in **bold**, second-best are underlined.

Task	Metric	Model	State	CZ	Wall	Heating
Total Load	NRMSE	LSTM-R	46.878 ± 2.981	47.926 ± 3.266	48.082 ± 2.152	46.546 ± 6.374
		Transformer-R	49.774 ± 3.372	50.574 ± 3.439	49.713 ± 2.575	48.527 ± 6.683
		TSMixer-R	42.892 ± 2.266	44.363 ± 2.189	44.959 ± 2.273	45.249 ± 2.324
		TimeXer-R	43.586 ± 5.288	47.884 ± 6.516	48.261 ± 6.209	47.554 ± 6.025
	CRPS	LSTM-R	0.197 ± 0.008	0.200 ± 0.006	0.180 ± 0.011	0.205 ± 0.023
		Transformer-R	0.203 ± 0.011	0.199 ± 0.005	0.184 ± 0.012	0.204 ± 0.029
		TSMixer-R	0.173 ± 0.006	0.175 ± 0.005	0.165 ± 0.009	0.166 ± 0.008
		TimeXer-R	<u>0.174 ± 0.022</u>	<u>0.186 ± 0.028</u>	<u>0.175 ± 0.027</u>	<u>0.172 ± 0.025</u>
HVAC Load	NRMSE	LSTM-R	44.099 ± 3.520	43.765 ± 4.692	44.201 ± 2.791	42.766 ± 6.457
		Transformer-R	44.780 ± 4.229	46.222 ± 5.158	44.535 ± 3.671	44.229 ± 6.876
		TSMixer-R	37.423 ± 1.994	36.405 ± 2.307	37.217 ± 1.738	38.855 ± 2.702
		TimeXer-R	38.814 ± 7.809	42.709 ± 10.206	43.136 ± 9.625	36.817 ± 2.572
	CRPS	LSTM-R	0.110 ± 0.006	0.105 ± 0.005	0.100 ± 0.011	0.111 ± 0.033
		Transformer-R	0.111 ± 0.009	0.109 ± 0.007	0.097 ± 0.012	0.112 ± 0.032
		TSMixer-R	0.098 ± 0.004	0.092 ± 0.004	0.085 ± 0.009	0.089 ± 0.010
		TimeXer-R	<u>0.100 ± 0.019</u>	<u>0.106 ± 0.025</u>	0.098 ± 0.025	0.083 ± 0.010
Temperature	NRMSE	LSTM-R	5.991 ± 0.546	6.108 ± 0.674	6.301 ± 1.122	7.009 ± 0.992
		Transformer-R	5.535 ± 0.401	5.317 ± 0.325	5.524 ± 0.329	4.642 ± 1.108
		TSMixer-R	<u>1.292 ± 0.036</u>	<u>1.348 ± 0.140</u>	<u>1.246 ± 0.096</u>	<u>1.341 ± 0.086</u>
		TimeXer-R	1.040 ± 0.031	1.102 ± 0.106	1.021 ± 0.091	1.098 ± 0.075
	CRPS	LSTM-R	2.410 ± 0.230	2.446 ± 0.256	2.537 ± 0.343	2.896 ± 0.433
		Transformer-R	2.156 ± 0.153	2.040 ± 0.115	2.142 ± 0.129	1.872 ± 0.392
		TSMixer-R	0.380 ± 0.006	0.412 ± 0.046	0.379 ± 0.030	0.411 ± 0.029
		TimeXer-R	0.263 ± 0.010	0.291 ± 0.036	0.271 ± 0.028	0.296 ± 0.024

For total and HVAC load forecasting, TSMixer-R consistently achieves the lowest NRMSE and CRPS across all domain categories, followed by TimeXer-R. The Wall construction domain yields the lowest CRPS for both tasks, consistent with its relatively low JS divergence values (Table 15), suggesting envelope-driven shifts are more structured. The Heating domain introduces the highest variance across models, indicating that heating technology shifts produce more heterogeneous cross-domain behavior. HVAC errors are consistently lower than total load errors because HVAC load is more tightly coupled to the weather features, and inherently have much lower variance compared to total loads. As load values are influenced by exogenous features, MLP-mixer model see those features multiple times when mixing, learning better dependence compared to a single attention operation.

Indoor temperature forecasting presents a different picture: TimeXer-R achieves the best accuracy, while LSTM-R and Transformer-R degrade by nearly an order of magnitude. TimeXer performs self attention on target, helping maintain the thermal inertia, and is still given some influence with token based cross-attention. This balances thermal inertia and exogenous influence better, which is what temperature dynamics require. This suggests cross-attention-based and mixer-style architectures better capture smooth, setpoint-driven thermal dynamics and exogenous driven load change better, respectively, under domain shift, whereas recurrent models and vanilla transformers without architectural conditioning of those exogenous features have high difficulty in generalizing across construction and climate changes. While intuitive, though not trivial or implied, we do also see a correlation in NRMSE and CRPS values - a model having one lower metric also has a lower other metric.

5.3 Zero-Shot Evaluation on Real data

We evaluate the robust model variants zero-shot on five real-world residential datasets — ECOBEE, HEAPO, IDEAL, NEST, and REFIT — consisting of all tasks and present the results in Table 6. We train on data split US States I (see section B) where 400 homes are sampled, to make up the training domain’s distribution for this experiment.

When tested on real data, we first observe that point forecast accuracy (NRMSE) degrades substantially relative to the synthetic domain evaluations, which is expected given the sim-to-real gap and the absence of any target-domain fine-tuning. TSMixer-R achieves the lowest NRMSE in six of eight columns, with TimeXer-R competitive on temperature tasks. Recurrent and vanilla transformer variants lag behind in generalizing to real data. This observation reinforces our observation made in previous experiment regarding Mixer style model aiding in seeing exogenous features more for load forecasting, and TimeXer finding a balance between self-attention and exogenous influence which is what temperature dynamics follow.

It is also observed that probabilistic performance has much greater success compared to point estimates. CRPS values are quite lower and more consistent across datasets, indicating that even without fine-tuning, models capture the general distributional shape of the target signal — including load spikes — quite better. This is quite consequential for downstream control and grid optimization tasks, where a calibrated predictive distribution is often more valuable than a sharp point estimate. TSMixer-R leads on CRPS for most total load and temperature columns, while TimeXer-R matches or surpasses it on HVAC load. Together, these results suggest that probabilistic pretraining on synthetic data transfers more readily than point forecast accuracy, motivating future work on distribution alignment methods to close the remaining sim-to-real gap.

Table 6: Real-data forecasting results grouped by target. Best values per column within each metric are **bolded**, second best underlined.

Metric	Model	Total Load				HVAC	Indoor Temperature		
		Heapo	Ideal	Nest	Refit	Nest	Ecobee	Ideal	Nest
NRMSE	LSTM-R	89.753	<u>97.706</u>	95.169	100.841	82.146	5.295	7.369	1.839
	Transformer-R	87.902	103.560	<u>96.067</u>	100.473	77.994	4.328	7.029	4.980
	TSMixer-R	75.595	92.272	95.718	88.860	<u>76.232</u>	<u>1.859</u>	3.687	1.614
	TimeXer-R	<u>81.335</u>	116.275	205.769	<u>99.296</u>	75.933	1.822	3.786	<u>1.626</u>
CRPS	LSTM-R	<u>0.182</u>	0.049	<u>0.023</u>	0.056	0.050	2.200	3.061	0.878
	Transformer-R	0.185	0.054	0.022	<u>0.057</u>	0.050	1.771	2.476	1.889
	TSMixer-R	0.169	<u>0.050</u>	0.031	0.060	<u>0.049</u>	<u>0.760</u>	1.448	0.719
	TimeXer-R	0.204	<u>0.096</u>	0.095	0.091	0.049	0.757	<u>1.465</u>	<u>0.761</u>

6 Limitations and Future Works

RESCAST-100K relies on physics-based simulation and still cannot fully replicate real occupant stochasticity and appliance heterogeneity — the primary driver of the sim-to-real gap observed in Section 5.3. But the goal, and the future works to address this, includes closer data alignment in the source dataset, which can be achieved through a learned or defined transfer utility function. Having a closer source distribution can aid in having a better prior for sim-to-real transfer. The included real-world datasets are also geographically limited and exhibit significant covariate missingness, motivating broader real-data integration in future releases. While the covariate missingness cannot be directly addressed, we aim to include more real datasets across further geographical locations for better understanding of real domain adaptation. The current benchmarks cover forecasting generalization and integration with downstream control tasks are natural extensions, which highly encourage users to pursue. The next version of RESCAST-100K also plans to include further building envelope details such as U-values, insulation values, etc. that can be used to benchmark physics informed and gray-box forecasting. The dataset also covers only U.S. residential stock; expanding to international building archetypes would broaden its scope, and require collaboration with different engineering fields.

7 Conclusion

We presented RESCAST-100K, a dataset of 15-minute resolution time series for 100,000 U.S. residential homes, pairing total load, HVAC load, and indoor temperature with exogenous weather signals, setpoints, and over 40 static building covariates. By integrating physics-based simulation with five curated real-world datasets under a unified schema and a configuration-based domain-split interface, RESCAST-100K enables rigorous, reproducible evaluation of transfer learning, domain adaptation, and zero-shot methods for residential forecasting — a class of evaluation no prior resource supported at this scale. Benchmarking six model families, we find that attention- and mixer-based architectures consistently outperform recurrent baselines under distribution shift, and that probabilistic pretraining on synthetic data transfers more reliably to real homes than point estimation. We release RESCAST-100K to support both the machine learning and building systems communities in advancing cross-domain residential forecasting.

References

- [1] Pecan street dataport, Apr 2025. URL <https://www.pecanstreet.org/dataport/>.
- [2] Rosemary E. Alden, Huangjie Gong, Cristinel Ababei, and Dan M. Ionel. Lstm forecasts for smart home electricity usage. In *2020 9th International Conference on Renewable Energy Research and Application (ICRERA)*, pages 434–438, 2020. doi: 10.1109/ICRERA49962.2020.9242804.
- [3] Zhiyu An, Xianzhong Ding, Arya Rathee, and Wan Du. Clue: Safe model-based rl hvac control using epistemic uncertainty estimation. *BuildSys ’23*, page 149–158, New York, NY, USA, 2023. Association for Computing Machinery. ISBN 9798400702303. doi: 10.1145/3600100.3623742.
- [4] Anestis Antoniadis, Solenne Gaucher, and Yannig Goude. Hierarchical transfer learning with applications to electricity load forecasting. *International Journal of Forecasting*, 40(2):641–660, 2024.
- [5] ASHRAE. ANSI/ASHRAE Standard 140-2023: Method of Test for Evaluating Building Performance Simulation Software. Technical report, American Society of Heating, Refrigerating and Air-Conditioning Engineers, Atlanta, GA, 2023.
- [6] Anaïs Berkes, Yoshua Bengio, David Rolnick, and Donna Vakalis. A hot dataset: 150,000 buildings for hvac operations transfer research. In *Proceedings of the 12th ACM International Conference on Systems for Energy-Efficient Buildings, Cities, and Transportation, BuildSys ’25*, page 171–180, New York, NY, USA, 2025. Association for Computing Machinery. ISBN 9798400719455. doi: 10.1145/3736425.3770110.
- [7] Tobias Brudermueller, Elgar Fleisch, Marina González Vayá, and Thorsten Staake. Heapo – an open dataset for heat pump optimization with smart electricity meter data and on-site inspection protocols. In *Proceedings of the 16th ACM International Conference on Future and Sustainable Energy Systems, E-Energy ’25*, page 699–711, New York, NY, USA, 2025. Association for Computing Machinery. ISBN 9798400711251. doi: 10.1145/3679240.3734637.
- [8] Long Cai, Jie Gu, and Zhijian Jin. Two-layer transfer-learning-based architecture for short-term load forecasting. *IEEE Transactions on Industrial Informatics*, 16(3):1722–1732, 2019.
- [9] Enrico Casella, Simone Silvestri, D. A. Baker, and Sajal K. Das. A human-centered power conservation framework based on reverse auction theory and machine learning. *ACM Trans. Cyber-Phys. Syst.*, 8(3), July 2024. ISSN 2378-962X. doi: 10.1145/3656348.
- [10] Jianli Chen, Rajendra Adhikari, Eric Wilson, Joseph Robertson, Anthony Fontanini, Ben Polly, and Opeoluwa Olawale. Stochastic simulation of occupant-driven energy use in a bottom-up residential building stock model. *Applied Energy*, 325:119890, 2022. ISSN 0306-2619. doi: <https://doi.org/10.1016/j.apenergy.2022.119890>.
- [11] Si-An Chen, Chun-Liang Li, Nathanael C. Yoder, Serkan O. Arik, and Tomas Pfister. Tsmixer: An all-mlp architecture for time series forecasting. *Transactions on Machine Learning Research (TMLR)*, 2023.
- [12] Michael Chesser, Padraic O’Reilly, Padraig Lyons, and Paula Carroll. The impact of extreme weather on peak electricity demand from homes heated by air source heat pumps. *Energy Sources, Part B: Economics, Planning, and Policy*, 16(8):707–718, 2021.

- [13] Davide Coraci, Silvio Brandi, Tianzhen Hong, and Alfonso Capozzoli. Online transfer learning strategy for enhancing the scalability and deployment of deep reinforcement learning control in smart buildings. *Applied Energy*, 333, 01 2023. ISSN ISSN 0306-2619. doi: 10.1016/j.apenergy.2022.120598. URL <https://www.osti.gov/biblio/1984646>.
- [14] Shijon Das, Mostafa M. Fouda, and Mohammad G. Abdo. Short-term load forecasting using gru-lgbm fusion. In *2024 International Conference on Smart Applications, Communications and Networking (SmartNets)*, pages 1–6, 2024. doi: 10.1109/SmartNets61466.2024.10577637.
- [15] Hengfang Deng, David Fannon, and Matthew J. Eckelman. Predictive modeling for us commercial building energy use: A comparison of existing statistical and machine learning algorithms using cbeccs microdata. *Energy and Buildings*, 163:34–43, 2018. ISSN 0378-7788. doi: <https://doi.org/10.1016/j.enbuild.2017.12.031>.
- [16] Jainam J. Dhruva and Simone Silvestri. Surrogate-assisted adaptive evolutionary algorithm for efficient hvac control in home energy management systems. *IEEE Access*, 14:56010–56025, 2026. doi: 10.1109/ACCESS.2026.3682562.
- [17] Patrick Emami, Abhijeet Sahu, and Peter Graf. Buildingsbench: A large-scale dataset of 900k buildings and benchmark for short-term load forecasting. In *Thirty-seventh Conference on Neural Information Processing Systems Datasets and Benchmarks Track*, 2023.
- [18] Xi Fang, Guangcai Gong, Guannan Li, Liang Chun, Pei Peng, and Xing Shi. Transferability investigation of a sim2real deep transfer learning framework for cross-building energy prediction. *Energy and Buildings*, 287:112968, 2023. ISSN 0378-7788. doi: <https://doi.org/10.1016/j.enbuild.2023.112968>.
- [19] Zhen Fang, Nicolas Crimier, Lisa Scanu, Alphanie Midelet, Amr Alyafi, and Benoit Delinchant. Multi-zone indoor temperature prediction with lstm-based sequence to sequence model. *Energy and Buildings*, 245:111053, 2021. doi: 10.1016/j.enbuild.2021.111053.
- [20] Chelsea Finn, Pieter Abbeel, and Sergey Levine. Model-agnostic meta-learning for fast adaptation of deep networks. In *International conference on machine learning*, pages 1126–1135. PMLR, 2017.
- [21] Steven Firth, Tom Kane, Vanda Dimitriou, Tarek Hassan, Farid Fouchal, Michael Coleman, and Lynda Webb. REFIT Smart Home dataset. 6 2017. doi: 10.17028/rd.lboro.2070091.v1. URL https://repository.lboro.ac.uk/articles/dataset/REFIT_Smart_Home_dataset/2070091.
- [22] Nan Gao, Wei Shao, Mohammad Saiedur Rahaman, Jun Zhai, Klaus David, and Flora D. Salim. Transfer learning for thermal comfort prediction in multiple cities. *Building and Environment*, 195:107725, 2021. ISSN 0360-1323. doi: <https://doi.org/10.1016/j.buildenv.2021.107725>.
- [23] Gargya Gokhale, Jonas Van Gompel, Bert Claessens, and Chris Develder. Transfer learning in transformer-based demand forecasting for home energy management system. BuildSys '23, page 458–462, New York, NY, USA, 2023. Association for Computing Machinery. ISBN 9798400702303. doi: 10.1145/3600100.3626635.
- [24] Yu He, Fengji Luo, and Gianluca Ranzi. Transferrable model-agnostic meta-learning for short-term household load forecasting with limited training data. *IEEE Transactions on Power Systems*, 37(4):3177–3180, 2022. doi: 10.1109/TPWRS.2022.3169389.
- [25] Georges Hebrail and Alice Berard. Individual Household Electric Power Consumption. UCI Machine Learning Repository, 2006. DOI: <https://doi.org/10.24432/C58K54>.
- [26] Philipp Heer, Curdin Derungs, Benjamin Huber, Felix Bünning, Reto Fricker, Sascha Stoller, and Björn Niesen. Comprehensive energy demand and usage data for building automation. *Scientific Data*, 11(1):469, May 2024. ISSN 2052-4463. doi: 10.1038/s41597-024-03292-2. URL <https://doi.org/10.1038/s41597-024-03292-2>.
- [27] Sepp Hochreiter and Jürgen Schmidhuber. Long short-term memory. *Neural Comput.*, 9(8): 1735–1780, November 1997. ISSN 0899-7667. doi: 10.1162/neco.1997.9.8.1735.
- [28] Josh Kace, Travis Walter, and Earth Advantage. Building performance database. Open Energy Data Initiative (OEDI), Office of Energy Efficiency & Renewable Energy, <https://data.openei.org/submissions/145>, 2014. URL <https://data.openei.org/submissions/145>. Accessed: 2026-04-29.

- [29] Christoph Klemenjak, Christoph Kovatsch, Manuel Herold, and Wilfried Elmenreich. A synthetic energy dataset for non-intrusive load monitoring in households. *Scientific data*, 7(1): 108, 2020.
- [30] Stephen J Lee and Cailinn Drouin. Forecasting residential heating and electricity demand with scalable, high-resolution, open-source models. *arXiv preprint arXiv:2505.22873*, 2025.
- [31] Han Li, Giuseppe Pinto, Alfonso Capozzoli, and Tianzhen Hong. Building thermal dynamics modeling with deep learning exploiting large residential smart thermostat dataset. In *Proceedings of the 9th ACM International Conference on Systems for Energy-Efficient Buildings, Cities, and Transportation*, pages 242–245, 2022.
- [32] Paulo Lissa, Michael Schukat, Marcus Keane, and Enda Barrett. Transfer learning applied to drl-based heat pump control to leverage microgrid energy efficiency. *Smart Energy*, 3:100044, 2021.
- [33] Na Luo and Tianzhen Hong. Lawrence berkeley national lab building 59, 01 2021. URL <https://www.osti.gov/biblio/1762808>.
- [34] Na Luo and Tianzhen Hong. Ecobee donate your data 1,000 homes in 2017, 03 2022. URL <https://www.osti.gov/biblio/1854924>.
- [35] Clayton Miller and Forrest Meggers. The building data genome project: An open, public data set from non-residential building electrical meters. *Energy Procedia*, 122:439 – 444, 2017. ISSN 1876-6102. doi: <https://doi.org/10.1016/j.egypro.2017.07.400>. {CISBAT} 2017 International Conference Future Buildings & Districts – Energy Efficiency from Nano to Urban Scale.
- [36] Clayton Miller, Anjukan Kathirgamanathan, Bianca Picchetti, Pandarasamy Arjunan, June Young Park, Zoltan Nagy, Paul Raftery, Brodie W. Hobson, Zixiao Shi, and Forrest Meggers. The building data genome project 2, energy meter data from the ashrae great energy predictor iii competition. *Scientific Data*, 7(1), Oct 2020. doi: 10.1038/s41597-020-00712-x.
- [37] Ozan Baris Mulayim, Pengrui Quan, Liying Han, Xiaomin Ouyang, Dezhi Hong, Mario Bergés, and Mani Srivastava. Are time series foundation models ready to revolutionize predictive building analytics? In *Proceedings of the 11th ACM International Conference on Systems for Energy-Efficient Buildings, Cities, and Transportation*, pages 169–173, 2024.
- [38] Alexander Neubauer, Mengbo Yu, Pedram Babakhani, Stefan Brandt, and Martin Kriegel. Transfer learning and explainable ai for heating load forecasting: A large-scale benchmark with shap-based static features. *Energy and AI*, page 100722, 2026.
- [39] Yuqi Nie, Nam H. Nguyen, Phanwadee Sinthong, and Jayant Kalagnanam. A time series is worth 64 words: Long-term forecasting with transformers. In *International Conference on Learning Representations (ICLR)*, 2023.
- [40] National Renewable Energy Laboratory (NREL). Energyplus™, 09 2017. URL <https://www.osti.gov/biblio/1395882>.
- [41] Andrew Parker, Henry Horsey, Matthew Dahlhausen, Marlena Praprost, Christopher CaraDonna, Amy LeBar, and Lauren Klun. Comstock reference documentation (v.1). Technical report, National Renewable Energy Laboratory (NREL), Golden, CO (United States), 03 2023. URL <https://www.osti.gov/biblio/1967948>.
- [42] Fang Peng, Tao Su, Qing Zeng, and Xiaojuan Han. Climate-adaptive energy forecasting in green buildings via attention-enhanced seq2seq transfer learning. *Scientific Reports*, 15(1): 31829, 2025.
- [43] Arian Prabowo, Xiachong Lin, Imran Razzak, Hao Xue, Emily W Yap, Matthew Amos, and Flora D Salim. Building timeseries dataset: Empowering large-scale building analytics. *Advances in Neural Information Processing Systems*, 37:133180–133206, 2024.
- [44] Martin Pullinger, Jonathan Kilgour, Nigel Goddard, Niklas Berliner, Lynda Webb, Myroslava Dzikovska, Heather Lovell, Janek Mann, Charles Sutton, Janette Webb, et al. The ideal household energy dataset, electricity, gas, contextual sensor data and survey data for 255 uk homes. *Scientific Data*, 8(1):146, 2021.
- [45] Heng Quan and Semiha Ergan. Sim-to-real transfer learning for large-scale short-term building energy forecasting in sustainable cities. *BuildSys '25*, page 86–95, New York, NY, USA, 2025. Association for Computing Machinery. ISBN 9798400719455. doi: 10.1145/3736425.3772006.

- [46] Fabian Raisch, Thomas Krug, Christoph Goebel, and Benjamin Tischler. Gentl: A general transfer learning model for building thermal dynamics. In *Proceedings of the 16th ACM International Conference on Future and Sustainable Energy Systems (E-Energy)*, 2025. doi: 10.1145/3679240.3734589.
- [47] Sufiyan Rehman. London Low Carbon Dataset. 8 2025. doi: 10.6084/m9.figshare.29983723.v2. URL https://figshare.com/articles/dataset/London_Low_Carbon_Dataset/29983723.
- [48] Abhinav Sagar. Smart building temperature forecasting with probabilistic temporal fusion transformers. In *UrbanAI: Harnessing Artificial Intelligence for Smart Cities*, Dec 2025.
- [49] Franco Scarselli, Marco Gori, Ah Chung Tsoi, Markus Hagenbuchner, and Gabriele Monfardini. The graph neural network model. *IEEE Transactions on Neural Networks*, 20(1):61–80, 2009. doi: 10.1109/TNN.2008.2005605.
- [50] Chen Shao, Michael Färber, Sebastian Pütz, Benjamin Schäfer, Yue Wang, Tobias Käfer, Zhanbo Huang, and Zhenyi Zhu. Real-e: A foundation benchmark for advancing robust and generalizable electricity forecasting. In *Proceedings of the 34th ACM International Conference on Information and Knowledge Management, CIKM '25*, page 6523–6527, New York, NY, USA, 2025. Association for Computing Machinery. ISBN 9798400720406. doi: 10.1145/3746252.3761637.
- [51] Andrew Speake, Eric Wilson, Yueyue Zhou, and Scott Horowitz. Resstock: Annual baseline results with component loads. Open Energy Data Initiative (OEDI), National Renewable Energy Lab, <https://doi.org/10.25984/2001060>, 2023. URL <https://data.openei.org/submissions/5959>. Accessed: 2026-04-28.
- [52] Swapna Thorve, Young Yun Baek, Samarth Swarup, Henning Mortveit, Achla Marathe, Anil Vullikanti, and Madhav Marathe. High resolution synthetic residential energy use profiles for the united states. *Scientific Data*, 10(1):76, 2023.
- [53] Artur Trindade. ElectricityLoadDiagrams20112014. UCI Machine Learning Repository, 2015. DOI: <https://doi.org/10.24432/C58C86>.
- [54] U.S. Department of Energy. Building america climate-specific guidance, n.d. URL <https://www.energy.gov/cmei/buildings/building-america-climate-specific-guidance>. Accessed: 2026-05-06.
- [55] Ashish Vaswani, Noam Shazeer, Niki Parmar, Jakob Uszkoreit, Llion Jones, Aidan N. Gomez, Łukasz Kaiser, and Illia Polosukhin. Attention is all you need. In *Advances in Neural Information Processing Systems (NeurIPS)*, 2017.
- [56] Yuxuan Wang, Haixu Wu, Jiexiang Dong, Guo Qin, Haoran Zhang, Yong Liu, Yunzhong Qiu, Jianmin Wang, and Mingsheng Long. Timexer: Empowering transformers for time series forecasting with exogenous variables. In *Advances in Neural Information Processing Systems (NeurIPS)*, 2024.
- [57] Di Wu and Weixuan Lin. Efficient residential electric load forecasting via transfer learning and graph neural networks. *IEEE Transactions on Smart Grid*, 14(3):2423–2431, 2023. doi: 10.1109/TSG.2022.3208211.
- [58] Zhuoqun Xing, Yiqun Pan, Yiting Yang, Xiaolei Yuan, Yumin Liang, and Zhizhong Huang. Transfer learning integrating similarity analysis for short-term and long-term building energy consumption prediction. *Applied energy*, 365:123276, 2024.
- [59] Shichao Xu, Yixuan Wang, Yanzhi Wang, Zheng O’Neill, and Qi Zhu. One for many: Transfer learning for building hvac control. *BuildSys '20*, page 230–239, New York, NY, USA, 2020. Association for Computing Machinery. ISBN 9781450380614. doi: 10.1145/3408308.3427617.
- [60] Zack Xuereb Conti, Ruchi Choudhary, and Luca Magri. A physics-based domain adaptation framework for modeling and forecasting building energy systems. *Data-Centric Engineering*, 4: e10, 2023. doi: 10.1017/dce.2023.8.
- [61] Yanan Zhang, Gan Zhou, Zhan Liu, Li Huang, and Yucheng Ren. An adaptive transfer learning framework for data-scarce hvac power consumption forecasting. *IEEE Transactions on Sustainable Energy*, 15(4):2815–2825, 2024. doi: 10.1109/TSTE.2024.3444689.

- [62] Haoyi Zhou, Shanghang Zhang, Jieqi Peng, Shuai Zhang, Jianxin Li, Hui Xiong, and Wancai Zhang. Informer: Beyond efficient transformer for long sequence time-series forecasting. In *Proceedings of the AAAI conference on artificial intelligence*, volume 35, pages 11106–11115, 2021.

Appendix

A Static Home Properties

Each home in RESCAST-100K is described by a set of static covariates drawn from ResStock’s building stock characterization. These subset of covariates are selected to reflect attributes that are *accessible without expert intervention*: they correspond to information a homeowner can typically retrieve from thermostat interfaces, public records, or simple visual inspections—without requiring specialized equipment, energy audits, or engineering expertise. The full set is listed in Table 7.

Table 7: Static covariates included per home in RESCAST-100K, grouped by category.

Category	Properties
Climate & Geography	ASHRAE/IECC Climate Zone, Building America Climate Zone, Climate Zone 2A Split
Location	County Metro Status, PUMA, PUMA Metro Status, City, Latitude, Longitude
Building Geometry	Building Type, Attic Type, Foundation Type, Floor Area, Number of Stories, Garage, Number of Bedrooms, Number of Occupants, Multi-Family/Single Family
Envelope	Wall Type, Wall Exterior Finish, Door Type, Window Type, Window Areas, Interior Shading, Orientation, Neighbors
Insulation	Ceiling, Floor, Foundation Wall, Rim Joist, Roof, Slab, Wall
HVAC & Heating	Heating Fuel, Heating System Type, Heating Type and Fuel, Cooling System Type, Shared HVAC System
Vintage	Construction Vintage, Construction Vintage (ACS)

The covariates span roughly seven categories encoding the primary dimensions of heterogeneity in the U.S.residential stock. Except latitude and longitude, which are taken as numerical inputs, all other properties are considered categorical and encoded using an ordinal encoder. Envelope and insulation fields characterize the thermal properties of the building shell, and how they govern indoor temperature dynamics and HVAC load. HVAC and heating fields capture mechanism-level differences in control logic and efficiency. Vintage encodes era-specific construction practices correlated with insulation levels, air sealing, and equipment efficiency. All fields are stored in a single metadata file indexed by `blgdg_id`. For real datasets, only a subset of covariates is available; the data loader handles missingness by masking unavailable fields, consistent with the robust training objective in Equation. The code includes a complete data dictionary outlining all the values corresponding to the categorical values for each of the variables.

B Domains Used: Description and Motivation

We define domain categories along four axes: geography, climate, envelope construction, and heating technology. These categories are intended to induce meaningful distribution shifts while remaining interpretable. State-based domains capture regional variation in weather, housing stock, building codes, occupant behavior, and utility context. Climate-zone domains provide a physics-informed partition that directly affects HVAC operation, seasonal load profiles, and thermal response. Wall construction domains approximate envelope properties such as thermal mass, insulation practice, and infiltration pathways. Finally, heating-system domains capture mechanism-level shifts in control logic, efficiency, and weather sensitivity across heating technologies. Together, these serve as an example of diverse domains categories to thoroughly evaluate a domain adaptation methodology. The domains

are listed in Tables 9, 10, 11, and 12. The splits create at the beginning of our experimentations, to test the non-robust methods, are also detailed in Table 8

Each of these four domain categories corresponds to a distinct research community that has, in isolation, identified the corresponding shift as the dominant generalization barrier. **State- and region-level shifts** are the focus of utility-side and grid-side forecasting work, where the heterogeneity of weather, building codes, tariffs, and stock composition across regions has motivated cross-region transfer studies on smart-meter and aggregated-demand data [17, 8, 4, 14]. **Climate-zone shifts** are studied predominantly by the building science and HVAC controls communities, who treat the ASHRAE/IECC partition as the unified domain for thermal-response stratification and have repeatedly shown that models trained in one zone degrade in others without adaptation [6, 42, 22, 54]. **Construction- and envelope-type shifts** are studied by the thermal-dynamics modeling community, where wall assembly, insulation, and infiltration determine the dominant time constants of indoor temperature response, and where building-to-building TL is known to be highly sensitive to envelope mismatch [46, 31]. **Heating-equipment shifts** are increasingly studied by the electrification and grid-planning communities, motivated by the projected impact of widespread heat-pump adoption on winter peaks [30, 12] — where the COP-, control-, and weather-sensitivity profile of the heating technology determines forecast tractability. No prior dataset enables controlled study of all four and more, and hence requiring RESCAST-100K.

Table 8: Domains curated for representative U.S. states from all IECC climate zones for near-in-distribution evaluation of the forecasting models.

Data Split	States
US States I	HI, PR, FL, AZ, TX, GA, KY, NC, IL, CO, MN, ME, AK, ND

Table 9: State-based geographic domains.

Domain	Description	States
state_northeast	Northeast/Mid-Atlantic dense corridor with mixed HVAC regimes.	MA, CT, RI, NY, NJ, PA, MD, DE, DC, VA
state_midwest	Great Lakes and Upper Midwest; cold winters and heating-dominant dynamics.	MI, WI, IL, IN, OH, MN, IA
state_southeast	Humid Southeast; cooling-heavy with latent loads and long summers.	FL, GA, SC, NC, AL, MS, TN
state_south_central	South-Central and Gulf-adjacent states with hot summers and strong cooling peaks.	TX, OK, AR, LA, NM
state_mountain_west	Mountain and Intermountain West; dry air and large diurnal temperature swings.	CO, UT, ID, MT, WY, NV, AZ

Table 10: Climate-zone domains based on IECC/ASHRAE climate-zone groupings.

Domain	Description	Zones
cz_hot_humid	Hot-humid climates; cooling-dominant operation with humidity effects.	1A, 2A
cz_hot_or_mixed_dry	Hot-dry and mixed-dry climates; sensible loads and large diurnal swings.	2B, 3B, 4B
cz_marine	Marine climates; mild temperatures, narrow ranges, and distinct shoulder seasons.	3C, 4C
cz_mixed_humid	Mixed-humid climates; balanced heating and cooling, useful as common transfer sources.	3A, 4A
cz_cold_to_very_cold	Cold to very cold climates; heating-dominant regimes and winter dynamics.	5A, 5B, 6A, 6B, 7A

We compare the domain shifts across domains under each category. We compare the target values and outdoor temperature. While these are a great way to visualize the data distributions, they do not capture the complexity of time series due to factors such as dropping the time indices leading, failing to capture the rate of changes, the conditional distributions, and more. Nonetheless, they are a gateway to understanding those underlying distributions. The distributions are visualized in Figures 3, 5, and 6. We also quantify these use JS divergence in tables 13, 14, 15, and 16.

Table 11: Envelope-construction domains defined by wall type and exterior finish.

Domain	Description	Wall type	Exterior finish
wood_siding	Lightweight wood-framed envelope with faster thermal response.	Wood Frame	Vinyl Light; Wood Medium/Dark; Fiber-Cement Light
brick_veneer	Wood frame with brick veneer; moderate thermal mass and common archetype.	Wood Frame	Brick Medium/Dark; Brick Light
masonry_block	Masonry or concrete block walls with higher thermal mass and lag.	Concrete	Stucco Light; Stucco Medium/Dark
stucco	Stucco exteriors representing a regional envelope archetype shift.	Wood Frame	Stucco Light; Stucco Medium/Dark
structural_brick	Structural brick walls with full masonry, high thermal mass, and strong lag.	Brick	None; Stucco Light; Vinyl Light

Table 12: Heating-technology domains.

Domain	Description	Heating type and fuel
heat_electric_furnace	Electric furnace with forced-air distribution.	Electricity Electric Furnace
heat_hp_electric	Electric air-source and mini-split heat-pump homes with variable COP behavior.	Electricity ASHP; Electricity MSHP
heat_elec._resistance_zonal	Zonal electric resistance heating with high weather sensitivity.	Electricity Baseboard; Electricity Electric Wall Furnace
heat_electric_boiler	Electric boiler with hydronic distribution.	Electricity Electric Boiler

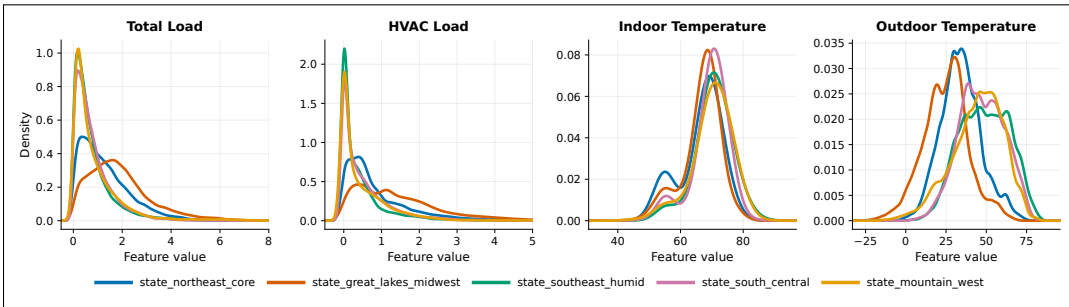


Figure 3: Distribution of total load, HVAC load, indoor and outdoor temperatures across state domains.

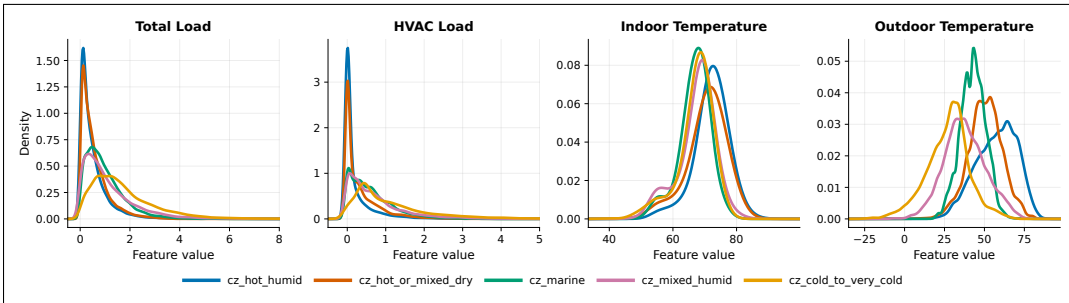


Figure 4: Distribution of total load, HVAC load, indoor and outdoor temperatures across climate zone domains.

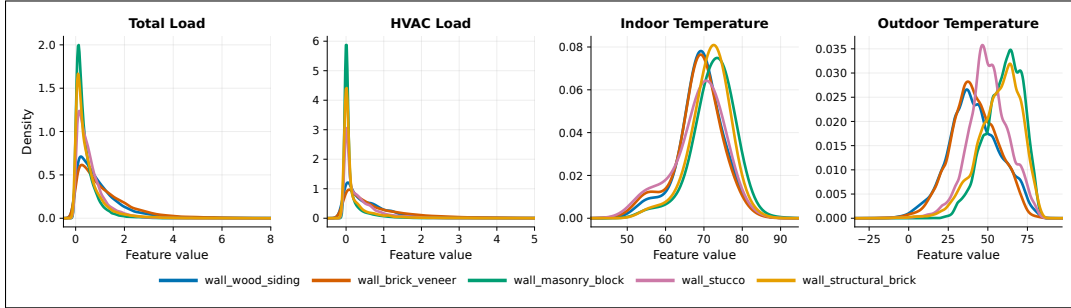


Figure 5: Distribution of total load, HVAC load, indoor and outdoor temperatures across different wall type domains.

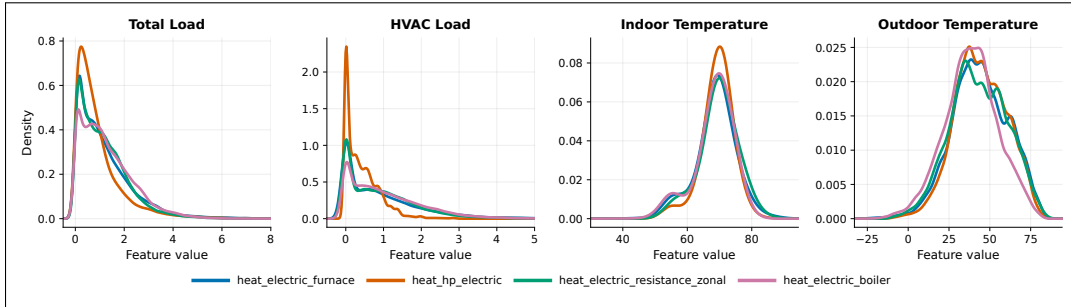


Figure 6: Distribution of total load, HVAC load, indoor and outdoor temperatures across heating equipment domains.

Table 13: JS Divergence between state domains.

Source Domain	Target Domain	Total Load	HVAC Load	Indoor Temp	Outdoor Temp
northeast_core	g._lakes_midwest	0.0363	0.0504	0.0489	0.0690
northeast_core	southeast_humid	0.0518	0.0790	0.1145	0.1285
northeast_core	south_central	0.0410	0.0457	0.0748	0.1119
northeast_core	mountain_west	0.0484	0.0756	0.1366	0.0965
g._lakes_midwest	southeast_humid	0.1542	0.1792	0.1400	0.2585
g._lakes_midwest	south_central	0.1403	0.1331	0.1150	0.2480
g._lakes_midwest	mountain_west	0.1350	0.1559	0.1524	0.1950
southeast_humid	south_central	0.0031	0.0110	0.0348	0.0100
southeast_humid	mountain_west	0.0068	0.0103	0.0212	0.0292
south_central	mountain_west	0.0101	0.0103	0.0447	0.0186

Table 14: JS Divergence between climate zone domains.

Source Domain	Target Domain	Total Load	HVAC Load	Indoor Temp	Outdoor Temp
hot_humid	hot_or_mixed_dry	0.0074	0.0205	0.0394	0.0650
hot_humid	marine	0.0818	0.1309	0.2553	0.2330
hot_humid	mixed_humid	0.0762	0.1283	0.2067	0.2286
hot_humid	cold_to_very_cold	0.2074	0.2440	0.2726	0.4134
hot_or_mixed_dry	marine	0.0533	0.0579	0.1641	0.1038
hot_or_mixed_dry	mixed_humid	0.0597	0.0607	0.1146	0.1387
hot_or_mixed_dry	cold_to_very_cold	0.1810	0.1630	0.1694	0.3411
marine	mixed_humid	0.0145	0.0092	0.0452	0.0931
marine	cold_to_very_cold	0.0634	0.0584	0.0516	0.2466
mixed_humid	cold_to_very_cold	0.0460	0.0463	0.0403	0.0837

Table 15: JS Divergence between wall construction domains.

Source Domain	Target Domain	Total Load	HVAC Load	Indoor Temp	Outdoor Temp
wood_siding	brick_veneer	0.0064	0.0112	0.0291	0.0077
wood_siding	masonry_block	0.0877	0.1189	0.1295	0.1830
wood_siding	stucco	0.0357	0.0332	0.0470	0.0615
wood_siding	structural_brick	0.0555	0.0885	0.1041	0.1208
brick_veneer	masonry_block	0.1185	0.1601	0.1660	0.2022
brick_veneer	stucco	0.0606	0.0608	0.0581	0.0633
brick_veneer	structural_brick	0.0800	0.1253	0.1315	0.1385
masonry_block	stucco	0.0218	0.0427	0.0841	0.0798
masonry_block	structural_brick	0.0082	0.0058	0.0267	0.0131
stucco	structural_brick	0.0119	0.0281	0.0603	0.0448

Table 16: JS Divergence between heating system domains.

Source Domain	Target Domain	Total Load	HVAC Load	Indoor Temp	Outdoor Temp
electric_furnace	hp_electric	0.0168	0.0794	0.0247	0.0050
electric_furnace	elec._res._zonal	0.0039	0.0038	0.0213	0.0065
electric_furnace	electric_boiler	0.0087	0.0105	0.0479	0.0170
hp_electric	elec._res._zonal	0.0188	0.0848	0.0408	0.0072
hp_electric	electric_boiler	0.0293	0.0980	0.0394	0.0207
elec._res._zonal	electric_boiler	0.0065	0.0081	0.0555	0.0149

C Loss function, Evaluation Metric, and Masking Details

This appendix specifies some of the components of Section 4 and Section 5: the training loss $\mathcal{L}_{\text{prob}}$, the evaluation metrics, and the masking distribution \mathcal{P}_M .

C.1 Probabilistic Loss

Let $\rho_\tau(\hat{q}, y) = (\tau - \mathbb{1}[y < \hat{q}])(\hat{q} - y)$ denote the pinball (quantile) loss at level $\tau \in (0, 1)$. Given a predicted quantile tensor $\hat{\mathbf{Q}}_\theta \in \mathbb{R}^{L_f \times Q}$ from Eq. (1) and ground truth $\mathbf{y}_{1:L_f}$, we define the training loss as the average pinball loss over horizon steps and quantile levels:

$$\mathcal{L}_{\text{prob}}(\hat{\mathbf{Q}}_\theta, \mathbf{y}_{1:L_f}) = \frac{1}{L_f \cdot Q} \sum_{t=1}^{L_f} \sum_{q=1}^Q \rho_{\tau_q}(\hat{Q}_{t,\tau_q}, y_t). \quad (5)$$

We use $Q = 10$ quantile levels uniformly spaced on $[0.05, 0.95]$, i.e. $\tau_q \in \{0.05, 0.15, \dots, 0.95\}$.

C.2 Evaluation Metrics

NRMSE measures point forecast accuracy by computing the root mean squared error normalized by the mean of the target variable, making it comparable across tasks with different scales:

$$\text{NRMSE} = \frac{\sqrt{\frac{1}{L_f} \sum_{t=1}^{L_f} (\hat{y}_t - y_t)^2}}{\bar{y}} \times 100, \quad (6)$$

where \hat{y}_t is the predicted value, y_t is the ground truth, and \bar{y} is the mean of the target series. CRPS evaluates probabilistic forecast quality by measuring the compatibility of a predicted distribution with an observed outcome, rewarding both calibration and sharpness. Since our model outputs a finite set of quantile predictions, we approximate CRPS via the sum of pinball losses across quantile levels:

$$\text{CRPS} \approx \frac{2}{L_f \cdot Q} \sum_{t=1}^{L_f} \sum_{q=1}^Q \rho_{\tau_q}(\hat{Q}_{t,\tau_q}, y_t), \quad (7)$$

where τ_1, \dots, τ_Q are the quantile levels and $\rho_\tau(z, y) = (\tau - \mathbb{1}[y < z])(z - y)$ is the pinball loss at quantile level τ . In all our experiments we use 10 quantiles uniformly spread between $[0.05, 0.95]$.

C.3 Masking Operator

To evaluate robustness to incomplete sensing, we introduce a structured masking operator that randomly removes subsets of input covariates before they are passed to the model. The goal is to simulate realistic missing-data conditions: in residential energy systems, weather feeds may be unavailable, thermostat or HVAC setpoint measurements may be missing, and static home attributes may be partially observed or unavailable. Rather than masking individual entries independently, our operator masks semantically meaningful groups of variables, making it closer to real conditions.

We partition the dynamic-input channels into weather and setpoint sub-blocks. Writing $\mathbf{x}_{1:L_c} = [\mathbf{y}_{1:L_c}; \mathbf{w}_{1:L_c}; \mathbf{h}_{1:L_c}]$ and $\mathbf{u}_{1:L_f} = [\mathbf{w}_{1:L_f}; \mathbf{h}_{1:L_f}]$, where \mathbf{w} stacks the N_w weather channels and \mathbf{h} stacks the N_h HVAC setpoint channels, the masking operator

$$\mathcal{M} : (\mathbf{x}_{1:L_c}, \mathbf{u}_{1:L_f}, \mathbf{s}) \mapsto (\tilde{\mathbf{x}}_{1:L_c}, \tilde{\mathbf{u}}_{1:L_f}, \tilde{\mathbf{s}})$$

leaves the past target $\mathbf{y}_{1:L_c}$ untouched and acts on the remaining components as follows.

Weather channels. For each weather variable $j \in \{1, \dots, N_w\}$, we draw a single Bernoulli mask $z_j^w \sim \text{Bernoulli}(p_w)$ and apply it jointly to the past and future windows of that channel:

$$\tilde{\mathbf{w}}_{1:L_c,j} = (1 - z_j^w) \mathbf{w}_{1:L_c,j}, \quad \tilde{\mathbf{w}}_{1:L_f,j} = (1 - z_j^w) \mathbf{w}_{1:L_f,j}.$$

A channel is therefore either fully observed or fully unobserved across the entire $L_c + L_f$ window.

HVAC setpoints. Heating and cooling setpoints are masked in tandem. A single Bernoulli draw $z^h \sim \text{Bernoulli}(p_h)$ removes all N_h setpoint channels jointly across both the past and future windows when $z^h = 1$:

$$\tilde{\mathbf{h}}_{1:L_c} = (1 - z^h) \mathbf{h}_{1:L_c}, \quad \tilde{\mathbf{h}}_{1:L_f} = (1 - z^h) \mathbf{h}_{1:L_f}.$$

Static house properties. We partition the static-feature indices $\{1, \dots, N_s\}$ into a set of key attributes K and remaining attributes R . Key attributes — which encode information typically retrievable from a thermostat or property record — are dropped with low probability, while remaining attributes are dropped with higher probability:

$$z_i^s \sim \begin{cases} \text{Bernoulli}(p_{\text{key}}), & i \in K, \\ \text{Bernoulli}(p_{\text{other}}), & i \in R, \end{cases} \quad \tilde{s}_i = (1 - z_i^s) s_i.$$

Observation indicator. Alongside $(\tilde{\mathbf{x}}, \tilde{\mathbf{u}}, \tilde{\mathbf{s}})$, the model receives a binary observation indicator \mathbf{m} with $m = 1$ on observed entries and $m = 0$ on masked entries. This allows the model to distinguish genuinely missing inputs from valid observations rather than conflating either case with a numeric zero. Together, \mathcal{M} and \mathbf{m} form an operator for realistic deployment settings where sensors, forecasts, or building metadata are usually only partially available.

D Forecasting Model Suite

D.1 Model Families and Motivation

We evaluate a set of recurrent, attention-based, and modern long-horizon time-series models in order to connect model families commonly used in building analytics with those currently used in the machine learning forecasting community. Let $L = 384$ denote the historical context length and $H = 96$ denote the forecast horizon. At each prediction time, the model receives historical target values $y_{1:L}$, historical weather covariates $w_{1:L}$, historical HVAC setpoint covariates $u_{1:L}$, known future weather covariates $w_{L+1:L+H}$, known future HVAC setpoint covariates $u_{L+1:L+H}$, and static building attributes s when used by the model.

Encoder LSTM (LSTM-E). LSTM-E corresponds to the baseline encoder-only LSTM. It follows the classical many-to-one recurrent forecasting design: an LSTM encoder reads the past window and the final hidden state is mapped directly to the full forecast horizon. This architecture is included because encoder LSTMs remain a common baseline in building load and indoor temperature forecasting, and provide a simple recurrent reference point against which more structured encoder-decoder and attention models can be compared [46].

Encoder–Decoder LSTM (LSTM). LSTM uses an encoder–decoder LSTM structure: a bidirectional LSTM encoder summarizes the historical sequence and a decoder LSTM consumes known future covariates to produce one prediction per future time step. Static building properties are used to condition the encoded state. This model represents the stronger recurrent family often used in building analytics, where known future weather and control signals are naturally incorporated into the decoder [19].

Transformer. Transformer is an encoder–decoder Transformer in which past target, weather, and control covariates form the encoder sequence, while known future weather and control covariates form the decoder sequence. We include this model because self-attention is the standard reference architecture for sequence modeling in modern ML [55], and because its ability to model long-range temporal dependencies is relevant for building thermal and energy dynamics.

TimeXer. TimeXer is a recent forecasting architecture designed to combine endogenous temporal patches with exogenous covariate information [56] through modified cross attention. It is included to represent recent ML forecasting models that explicitly target prediction with external variables.

TSMixer. TSMixer uses MLP-style mixing across temporal and feature dimensions rather than recurrent or attention-based sequence processing [11]. We include it as a lightweight modern ML baseline, since mixer-style models often provide strong performance with lower architectural complexity.

PatchTST. PatchTST tokenizes time series into patches and applies Transformer-style modeling over patch tokens [39]. It is included because patch-based Transformers are a strong and widely used modern baseline for long-horizon time-series forecasting.

Together, these models bridge two communities: recurrent encoder and encoder–decoder models that are familiar in building analytics, and Transformer, patch-based, and mixer-based architectures that are now common in the broader ML time-series literature.

D.2 Robust Model Construction

We construct robust versions of selected models to handle unavailable covariates: LSTM-R, Transformer-R, TimeXer-R, and TSMixer-R. These models are chosen as they perform the best under in domain evaluation. Robustness is introduced through structured missingness augmentation and model-specific missing-value handling.

Structured missingness augmentation. During robust training, selected inputs are replaced with NaN. Each weather channel is masked across both historical and future windows with probability $p_w = 0.6$. The HVAC setpoint pair is masked jointly with probability $p_u = 0.9$. Static building properties are divided into key and non-key attributes: key attributes are retained with probability 0.9, while non-key attributes are dropped with probability 0.9. For unmasked models, this corruption operator is disabled.

For an input block $X \in \mathbb{R}^{T \times C}$, define the observation mask

$$M_{t,c} = \mathbf{1}\{X_{t,c} \text{ is finite}\}, \quad (8)$$

and the zero-filled value

$$\tilde{X}_{t,c} = M_{t,c} X_{t,c}. \quad (9)$$

NaN-aware tokenization for LSTM-R and Transformer-R. For LSTM-R and Transformer-R, each scalar variable is encoded together with its observation indicator:

$$e_{t,c} = \phi \left([\tilde{X}_{t,c}, M_{t,c}] \right) \in \mathbb{R}^d, \quad (10)$$

where ϕ is a two-layer MLP. The variable embeddings are then pooled with the observation mask:

$$z_t = \text{LN} \left(\frac{\sum_{c=1}^C M_{t,c} e_{t,c}}{\max \left(\sum_{c=1}^C M_{t,c}, 1 \right)} \right). \quad (11)$$

Thus unavailable variables receive zero weight, while the model is explicitly informed which values were observed.

LSTM-R. LSTM-R applies the NaN-aware tokenizer to both historical and future inputs,

$$X_t^p = [y_t, w_t, u_t], \quad X_h^f = [w_{L_c+h}, u_{L_c+h}], \quad (12)$$

for $h = 1, \dots, L_f$. A bidirectional LSTM encoder processes $z_{1:L_c}^p$, and a decoder LSTM processes $z_{1:L_f}^f$:

$$h_{L_c}, c_{L_c} = \text{BiLSTM}_{enc}(z_{1:L_c}^p), \quad (13)$$

$$d_{1:L_f} = \text{LSTM}_{dec}(z_{1:L_f}^f; h_{L_c}, c_{L_c}), \quad (14)$$

$$\hat{y}_{h,q} = W_q d_h + b_q. \quad (15)$$

Transformer-R. Transformer-R uses the same NaN-aware tokenization but replaces the recurrent encoder and decoder with Transformer blocks:

$$m_{1:L_c} = \text{TransformerEncoder}(z_{1:L_c}^p), \quad (16)$$

$$r_{1:L_f} = \text{TransformerDecoder}(z_{1:L_f}^f, m_{1:L_c}), \quad (17)$$

$$\hat{y}_{h,q} = W_q r_h + b_q. \quad (18)$$

No causal decoder mask is used because decoder inputs are known future covariates rather than future target values.

TimeXer-R and TSMixer-R. TimeXer-R and TSMixer-R use the same structured masking augmentation, but preserve the original backbone input interface by replacing non-finite values with a sentinel value:

$$X_{t,c}^{fill} = \begin{cases} X_{t,c}, & M_{t,c} = 1, \\ c, & M_{t,c} = 0. \end{cases} \quad (19)$$

This informs the backbone about unavailable covariates during training without changing the TimeXer or TSMixer architecture. TimeXer-R uses the same TimeXer backbone family but changes the robust configuration in two ways: it is trained with structured missingness, and it uses a shorter patch length ($p = 4$ instead of $p = 12$). The shorter patch length gives the model finer temporal resolution when forming endogenous tokens, which can help when missing covariates remove some of the exogenous context. TSMixer-R, in contrast, keeps the same mixer-style backbone and patch length as TSMixer. Its robustness comes only from the training distribution: during training, weather, HVAC, and static building covariates are randomly made unavailable, and missing entries are replaced by the model’s robust fill pathway before being passed to the mixer. Thus, TimeXer-R modifies both the training corruption process and the temporal tokenization granularity, whereas TSMixer-R isolates the effect of structured missingness training on an otherwise unchanged TSMixer backbone.

E Hyperparameters

Table outlines the model parameters for each model used in this work. For LSTM-E, the encoder-layer count refers to the stacked LSTM encoder and there is no decoder. For LSTM and LSTM-R, encoder and decoder layers refer to LSTM stacks; the “FFN/token dim” column denotes the hidden dimension used by the robust-capable variable tokenizer. For Transformer and Transformer-R, heads, encoder layers, decoder layers, and FFN dimension refer to standard Transformer blocks. TimeXer and PatchTST use attention over patched sequences, so patch length is applicable. TSMixer and TSMixer-R do not use attention heads or decoder layers, so these entries are marked with dashes.

Training hyperparameters. All neural models are trained with AdamW using learning rate 5×10^{-4} and weight decay 10^{-2} . We use cosine annealing over the full training run with minimum learning rate 10^{-4} , where the schedule length is the number of epochs multiplied by the number of training batches. Gradients are clipped to norm 1.0. Mixed-precision training is enabled on CUDA when supported. Unless otherwise specified, models are trained for 3 epochs, with batch sizes given in Table 17. The checkpoint with the best validation performance is retained for evaluation.

Table 17: Hyperparameters for the forecasting models. A dash indicates that the quantity is not applicable to that architecture.

Model	d_{model}	Heads	Enc. layers	Dec. layers	FFN/token dim	Dropout	L_c	L_f	Patch	Batch	Robust masking
LSTM-E	125	–	1	–	–	0.1	384	96	–	128	No
LSTM	256	–	1	1	256	0.1	384	96	–	128	No
Transformer	128	8	1	1	256	0.1	384	96	–	128	No
TimeXer	128	8	1	–	256	0.1	384	96	12	256	No
TSMixer	128	–	1	–	256	0.1	384	96	12	128	No
PatchTST	128	8	1	–	256	0.1	384	96	12	128	No
LSTM-R	128	–	1	1	256	0.1	384	96	–	256	Yes
Transformer-R	128	8	1	1	256	0.1	384	96	–	256	Yes
TimeXer-R	128	8	1	–	512	0.1	384	96	4	128	Yes
TSMixer-R	128	–	1	–	256	0.1	384	96	12	128	Yes

F Compute Information

Dataset generation and model training were performed on high performance compute environments. The EnergyPlus simulations for the 100k homes were executed on a high-performance computing cluster using 48x6 CPU cores across 6 nodes. Total simulation compute was approximately 100 CPU-hours. Model training and evaluation were performed on $4 \times$ V100 GPUs with 32 GB system memory. A single training run for the largest model (TimeXer-R) takes approximately 8 minutes per 3 epochs at batch size 128. Each zero-shot cross-domain evaluation (Section 5.2) requires approximately 8 GPU-minutes per source–target domain pair. The full set of experiments reported in Tables 4–6, including all robust and non-robust variants across the four domain categories and sim-to-real evaluations, required approximately 24 total GPU-hours. Preliminary experiments, failed experiments, and exploration not reported in the paper consumed an additional 300 CPU and 100 GPU hours.

G Synthetic to Real Motivation

Here we compare the distribution of real v/s synthetic datasets. We do this for indoor temperature values and total load values. We compare the distributions of values itself y_t , and the the first differences (Δy_t). For each dataset, we create a dataset with manual intervention. Considering geographical location and home size - we make a data split of synthetic homes. We compare the distribution of the real dataset and the curated synthetic dataset. We observe that the synthetic distributions are very similar to real datasets, hence providing stronger motivation for synthetic source domain alignment for better sim to real transfer.

Table 18: JS divergence across read datasets and corresponding synthetic splits.

Dataset	Location	Synthetic Split	Task	JS
ECOBEE	Across USA	All States	Temperature forecasting	0.1108
HEAPO	Canton of Zurich, Switzerland	MN WI MI	Total load forecasting	0.0491
IDEAL	United Kingdom	WA OR	Temperature forecasting	0.0630
IDEAL	United Kingdom	WA OR	Total load forecasting	0.0272
NEST	California, USA	CA	Temperature forecasting	0.1349
NEST	California, USA	CA	HVAC load forecasting	0.0871
NEST	California, USA	CA	Total load forecasting	0.1492
REFIT	United Kingdom	WA OR	Total load forecasting	0.0188

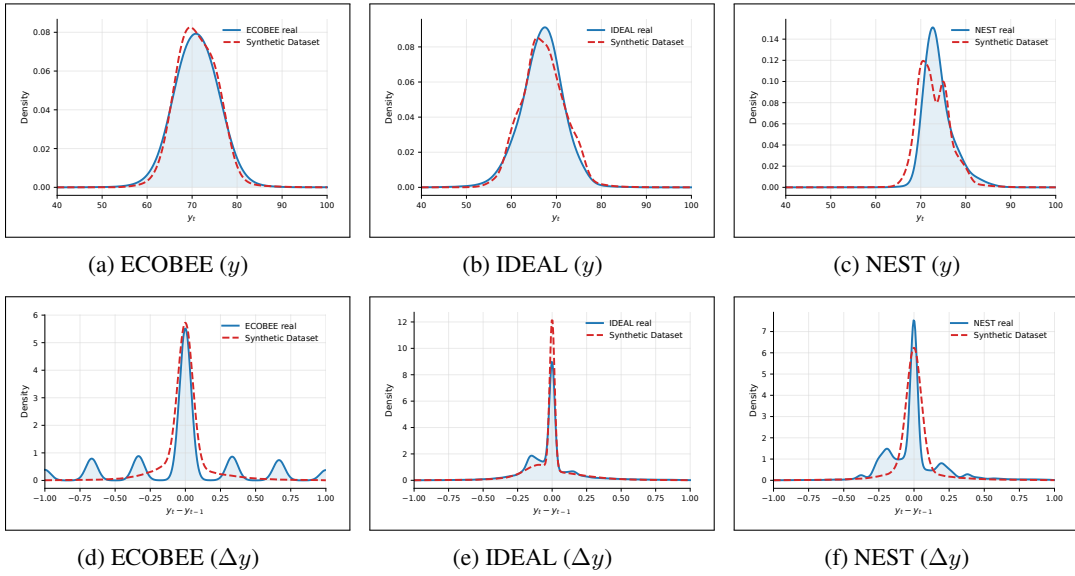


Figure 7: Distributions of indoor temperature values (y) in the top row and their consecutive differences (Δy) in the bottom row across real and their corresponding synthetic datasets.

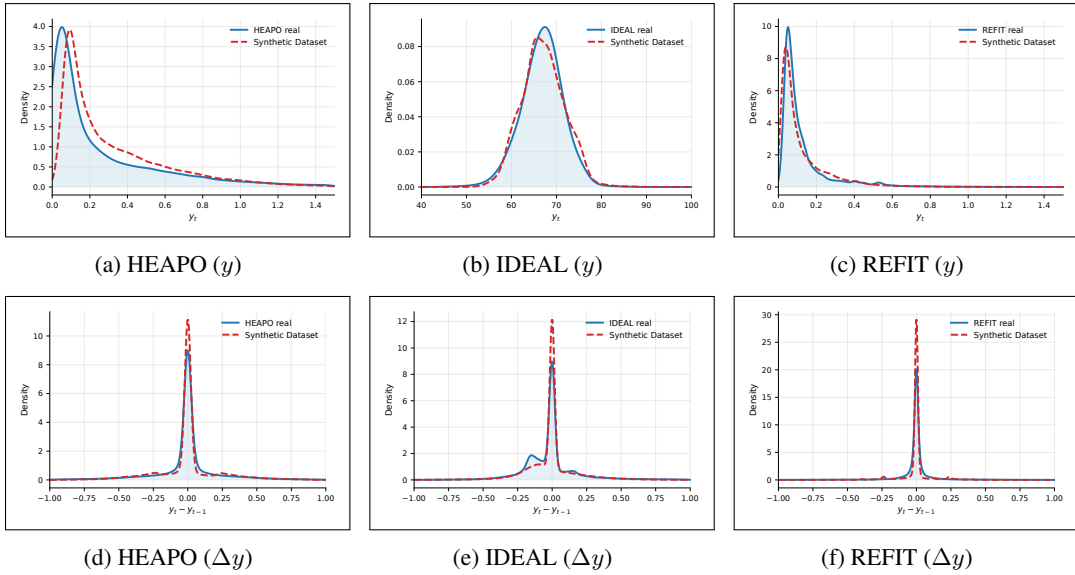


Figure 8: Distributions of total load values (y) in the top row and their consecutive differences (Δy) in the bottom row across real and their corresponding synthetic datasets.